Research Square

Preprints are preliminary reports that have not undergone peer review.
They should not be considered conclusive, used to inform clinical practice,
or referenced by the media as validated information.

# From Bulk Copper Samples to Functional DCB Test Boards: Process Transfer and Joint Characterization of Pressure-Less Nano-Silver Sintering

**Cheng Zhang**

cheng.zhang_jhu@hotmail.com

TU Chemnitz Fakultät für Maschinenbau https://orcid.org/0009-0009-7267-9300

**Matthias Tuerpe**

Dresden University of Technology: Technische Universitat Dresden

**Research Article**

**Keywords:** pressure-less sintering, nano-silver precursor paste, DCB test board, Cu-cube joint, four-terminal sensing, die shear testing

**Posted Date:** November 2nd, 2026

**DOI:** https://doi.org/10.21203/rs.3.rs-11120361/v1

**License:** This work is licensed under a Creative Commons Attribution 4.0 International License.
Read Full License

# Abstract

Increasing operating temperatures in power electronic applications require joining technologies with improved thermal and mechanical stability compared with conventional Sn-based soldering. Silver sintering is a promising alternative, but many sintering processes still require elevated temperatures and external pressure. Pressure-less sintering using in-situ nano-silver precursor pastes offers a potential route for low-temperature joining without applied joining pressure.

In this study, a pressure-less nano-Ag sintering process previously investigated on bulk copper samples was transferred to application-oriented direct copper bonding (DCB) test boards. A Cu-cube/DCB test structure was developed to enable four-terminal resistance measurement, die shear testing, metallographic analysis, and SEM characterization of the sintered joint region.

The as-joined Cu-cube/DCB joints showed low electrical resistance and shear strength values mainly in the range of 70–80 MPa. Metallographic analysis revealed a continuous Ag-based bonding layer between the Cu-cube and the DCB substrate. SEM observations showed a porous sintered Ag microstructure with local non-uniformities, especially near the edge regions. Fracture surface analysis indicated predominantly cohesive fracture within the sintered Ag layer, with local interfacial contributions.

Overall, the results demonstrate that precursor-based pressure-less nano-Ag sintering can be transferred from simplified bulk copper samples to functional DCB test boards. The Cu-cube/DCB configuration provides a suitable platform for electrical, microstructural, and mechanical assessment of pressure-less sintered Ag joints.


# 1 Introduction

Modern power electronic systems are continuously evolving toward higher power density and higher operating temperatures, especially in automotive applications [1, 2]. The increasing use of wide-bandgap semiconductors such as SiC and GaN further accelerates this trend, as these devices can operate at elevated junction temperatures [3]. Under such conditions, conventional Sn-based solder materials approach their performance limits, particularly with respect to thermal fatigue and long-term reliability under cyclic thermal loading [2, 4].

Silver sintering has therefore been widely investigated as an alternative joining technology due to its high thermal conductivity, excellent electrical conductivity, and high melting point [1, 5]. In addition, sintered silver joints can provide improved thermo-mechanical stability compared with conventional solder joints, making them suitable for high-temperature electronic packaging applications [2, 6]. However, conventional silver sintering processes often require elevated temperatures and external mechanical pressure to achieve sufficient densification and bonding strength. This increases process complexity and can limit industrial implementation, especially for pressure-sensitive components or complex assemblies [5, 7].

To overcome these limitations, pressure-less sintering approaches based on nano-silver materials have been developed in recent years [5, 8]. These approaches enable bonding at reduced temperatures without the application of external joining pressure, while maintaining promising mechanical and electrical performance [6, 8]. Among them, precursor-based nano-silver pastes are of particular interest. During thermal treatment, the precursor decomposes and generates nanoscale silver particles in situ. These newly formed particles promote sintering and support the formation of a metallic Ag network at relatively low processing temperatures [5, 9, 10].

The performance of sintered Ag joints is strongly influenced by their local microstructure. Previous studies have shown that neck formation, particle coalescence, porosity distribution, and local heterogeneity play an important role in the development of mechanical and electrical properties [6, 11–13]. Therefore, the evaluation of pressure-less sintered Ag joints should not only consider the joining strength, but also the morphology and continuity of the sintered Ag layer.

Despite significant progress, many studies on nano-Ag sintering are still based on simplified sample geometries, such as bulk copper substrates or model die-attach configurations [6, 8]. These systems are useful for investigating fundamental bonding behavior, but they only partially represent practical application conditions in electronic packaging. In particular, the transfer of pressure-less nano-Ag sintering processes to application-oriented substrate systems, such as direct copper bonding (DCB) test boards, remains an important step toward practical implementation [14, 15].

One important limitation of bulk copper samples is related to electrical characterization. Due to the high electrical conductivity and large volume of the surrounding copper material, the measured resistance is often dominated by the substrate itself. As a result, the resistance contribution of the sintered Ag joint cannot be sufficiently separated from the total measured resistance [8, 15, 17]. This makes it difficult to evaluate the electrical behavior of the joining layer under application-oriented conditions.

When moving from bulk materials to functional test boards, additional challenges arise from the substrate design, material combination, and joint geometry. Polymer-based test boards, such as FR4 or RF laminates, may be limited by their thermal stability during sintering. In contrast, DCB substrates provide higher thermal stability and are widely used in power electronic applications due to their copper/ceramic/copper structure [14, 16]. However, the transfer to DCB-based test structures requires suitable sample geometries that allow electrical resistance measurement, metallographic analysis, and mechanical assessment of the sintered joint region.

Therefore, there is a need to investigate pressure-less nano-Ag sintering on application-oriented test structures and to evaluate whether such configurations are suitable for combined electrical, microstructural, and mechanical characterization. Test boards designed for four-terminal sensing can provide a more defined measurement of the joint resistance, while metallographic and fracture surface analyses can provide insight into the morphology and failure appearance of the sintered Ag layer.

In this work, a commercially available in-situ nano-silver precursor paste is investigated with a focus on transferring the pressure-less sintering process from previously studied bulk copper samples to functional DCB test boards [17]. A Cu-cube/DCB test structure is developed to enable four-terminal electrical resistance measurement, light microscopy, SEM analysis, and die shear testing of the sintered joint region.

The objective of this study is to evaluate the suitability of the Cu-cube/DCB configuration for the as-joined characterization of pressure-less sintered Ag joints. The electrical resistance, cross-sectional morphology, local porosity, shear strength, and fracture surface appearance are analyzed. This study therefore contributes to bridging the gap between simplified material-level investigations and application-oriented test structures for power electronic packaging.

## 2 Materials and Methods

# 2.1 Nano-Ag Precursor Paste

A commercially available in-situ nano-silver precursor paste supplied by Nano-Join GmbH, Berlin, Germany, was used in this study. The paste contains a high silver content of more than 90 wt.% and consists of an organometallic silver precursor together with micron-sized silver particles. During thermal treatment, the precursor decomposes and generates nanoscale silver particles in situ. The generated nanoscale Ag contributes to the formation of a metallic sintered network during the pressure-less joining process.

The material characteristics and basic sintering behavior of this paste have been reported in previous work [17]. In the present study, the same material system was used for the transfer from bulk copper samples to functional test board structures.

# 2.2 Transfer Strategy from Bulk Copper Samples to Functional Test Boards

The transfer strategy used in this work is based on a methodological development approach that was previously presented [18], as illustrated in Fig. 1. This approach was adapted from the concept of joinability described in DIN 8514:2006-05 [19], in which the suitability of a joining technology is considered through the interaction between material, process, and design. For the pressure-less nano-Ag sintering process investigated here, this concept was transferred to three development stages: material suitability, process feasibility, and design-related joint reliability.

In the first stage, the material suitability of the in-situ nano-silver precursor paste was evaluated on copper substrates. Simplified copper samples, including sandwich and bending specimens, were used to verify whether the paste can form a metallic bond on copper surfaces at a maximum temperature of 250°C without external pressure. These experiments provided the basis for assessing the fundamental compatibility between the paste and copper surfaces [18].

In the second stage, the process feasibility was investigated using standard copper shear samples. This configuration allowed the influence of the sintering process on the joining behavior to be studied under defined conditions. The bulk copper samples therefore served as a reference system for evaluating the basic bonding capability and mechanical performance of the pressure-less sintered Ag joints, as reported in previous work [17, 18].

The present study focuses on the third stage of this development approach, namely the transfer of the process to functional test board structures. The aim of this stage is to move from simplified laboratory samples toward application-oriented configurations and to develop a test structure that allows electrical characterization, die shear testing, metallographic analysis, and SEM characterization of the sintered joint region on the same platform.

In the first transfer step, RF-35/FR4-based test boards were investigated as polymer-based circuit board structures. They allow the integration of defined electrical measurement paths and were therefore considered for the electrical characterization of pressure-less sintered Ag joints.

However, the limited thermal stability of the polymer-based board material restricted its suitability for the applied sintering profile. Under the selected thermal conditions, the bonding quality was not sufficient for systematic characterization. Therefore, the RF-35/FR4-based test boards were not selected as the final substrate platform.

As a next transfer step, DCB substrates were introduced because of their higher thermal stability and their relevance for power electronic applications. An initial DCB test board design was based on a Cu-bridge geometry, as shown in Fig. 2. This configuration allowed the realization of a defined electrical path and was suitable for four-terminal sensing.

However, the elongated Cu-bridge geometry introduced additional geometry-related constraints, including an increased influence of residual stresses. Therefore, this design was not selected as the final test structure.

The final test structure was simplified to a Cu-cube geometry on DCB substrates. In this configuration, the Cu-cube was bonded directly to the copper metallization of the DCB substrate using the in-situ nano-Ag precursor paste.

The Cu-cube/DCB configuration, shown in Fig. 3, provides a defined bonding area and a comparatively simple joint geometry. It enables four-terminal resistance measurement, die shear testing, metallographic cross-sectioning and SEM analysis of the same type of pressure-less sintered Ag joint. Therefore, this configuration was selected as the main test structure in the present study.

# 2.3 Pressure-less Sintering Process

Prior to sintering, the copper surfaces of the test boards and joining partners were prepared to ensure reproducible joining conditions. Surface oxides were removed using a citric acid solution. The samples

were then rinsed with ethanol to remove residues and dried under ambient conditions.

The in-situ nano-silver precursor paste was applied by stencil printing. The wet paste layer thickness was approximately 80 µm. After paste deposition, the Cu-cubes were positioned on the DCB test boards using a pick-and-place system in order to ensure controlled placement and contact at the joining interface.

The sintering process was carried out in a laboratory furnace under nitrogen atmosphere. The applied temperature profile is shown in Fig. 4. The samples were first heated from room temperature to approximately 100°C, followed by a short holding period of about 5 min. Subsequently, the temperature was increased to a peak temperature of 250°C. The heating rate was approximately 6°C·min$^{-1}$. The peak temperature was maintained for 60 min. After the dwell period, the samples were cooled naturally to room temperature.

In parallel with the temperature profile, the furnace ventilation was controlled to support the removal of gaseous decomposition products. At the beginning of the heating stage, the ventilation level was increased to approximately 50%. After the initial holding stage, it was reduced to approximately 35% and maintained during the main heating and dwell period. After approximately 120 min, the ventilation was increased to 100% and kept at this level during the final stage of the process.

The same sintering parameters as in previous studies [17, 20] were applied to the investigated Cu-cube/DCB samples in order to ensure comparability of the results.

## 2.4 Electrical Characterization

Electrical characterization was performed on the Cu-cube/DCB test boards using a four-terminal sensing method. The test board layout included separated current supply and voltage sensing paths. This configuration allows the resistance of the defined joint region to be measured with reduced influence from external contact resistance and surrounding copper traces.

During the measurement, current was applied through the outer electrodes, while the voltage drop was measured using the inner voltage sensing electrodes. The electrical resistance was calculated from the measured voltage drop and the applied current. Compared with the previously used bulk copper samples, this layout provides a more suitable configuration for evaluating the electrical behavior of the sintered Ag joint, as shown in Fig. 5.

All measurements were carried out at room temperature. For each selected sample, repeated measurements were performed at different measurement points. In the present study, at least five samples were investigated, with nine repeated measurements per sample. The repeated measurements were used to evaluate the reproducibility and statistical distribution of the measured resistance values.

## 2.5 Microstructural Characterization

Metallographic characterization was carried out to evaluate the morphology of the pressure-less sintered Ag joint between the Cu-cube and the DCB substrate. Selected samples were embedded, ground, and polished to prepare cross-sections through the joining area.

The prepared cross-sections were first examined by light microscopy using an Axio Imager.M2m microscope from Carl Zeiss, Germany. Light microscopy was used to evaluate the overall joint geometry, the continuity of the Ag-based bonding layer, and local variations in layer thickness.

Scanning electron microscopy (SEM) was then used to analyze the sintered Ag layer in more detail. SEM observations focused on the morphology of the sintered Ag network, local porosity, and microstructural non-uniformities within the joining layer. The SEM investigations were carried out using a Sigma 360 VP scanning electron microscope from Zeiss, Germany.

## 2.6 Die Shear Testing and Fracture Surface Analysis

Die shear testing was performed to evaluate the mechanical performance of the Cu-cube/DCB joints in the as-joined condition. The tests were carried out using an adapted shear fixture installed in a conventional universal testing machine (ZwickRoell Z010, ZwickRoell GmbH & Co. KG, Germany). During testing, the DCB test board was fixed in the fixture to prevent movement, while the shear tool was positioned close to the joining interface of the Cu-cube.

The shear tool was moved laterally against the Cu-cube until failure of the joint occurred. The maximum shear force recorded during the test was used to calculate the shear strength. The shear strength was determined by dividing the maximum shear force by the bonded area of the Cu-cube [18].

After die shear testing, the fracture surfaces were examined by SEM. Both the Cu-cube side and the DCB-testboard side were analyzed in order to identify the fracture appearance and the distribution of residual sintered Ag. The fracture surface analysis was used to distinguish between adhesive and cohesive fracture within the sintered Ag joining layer.

# 3 Results and Discussion

This section evaluates the as-joined Cu-cube/DCB joints prepared by pressure-less nano-Ag sintering. The focus is placed on electrical resistance measurement, metallographic analysis, SEM characterization, die shear testing, and fracture surface analysis.

The results are presented in three parts. First, the electrical resistance of the as-joined Cu-cube joints is evaluated using four-terminal sensing. Second, the cross-sectional morphology and local microstructure of the sintered Ag layer are analyzed by light microscopy and SEM. Finally, die shear testing and fracture surface analysis are used to assess the mechanical performance and failure appearance of the as-joined joints.

## 3.1 Electrical Characterization of Cu-cube Joints

The electrical resistance of the as-joined Cu-cube joints was measured using the four-terminal sensing method described in Section 2.4. The measured resistance values are shown in Fig. 6. The box plots show the distribution of the repeated measurements for eight selected Cu-cube joints.

The resistance values are generally in a low resistance range between approximately 0.055 mΩ and 0.070 mΩ. Most samples show values concentrated between approximately 0.062 mΩ and 0.069 mΩ. This confirms that the pressure-less sintered Ag joints are electrically conductive in the as-joined condition.

The mean values, marked by diamond symbols, are close to the corresponding median values for most samples. This indicates that the repeated measurements show a relatively stable distribution. Samples 4, 5, and 7 exhibit comparatively higher resistance values, while samples 6 and 8 show lower resistance values. Sample 7 shows a broader distribution compared with the other samples, indicating larger variation between the repeated measurement points. In contrast, samples 2, 4, 5, and 8 show relatively narrow distributions.

The measured values should be interpreted as the resistance of the defined joint region between the voltage sensing points. They should not be considered as the intrinsic resistivity of the sintered Ag layer, because the effective current path and the exact joint cross-section cannot be determined precisely from the present measurement configuration.

Overall, the four-terminal measurements show that the Cu-cube/DCB test board layout enables reproducible resistance measurement of the pressure-less sintered Ag joints. The as-joined joints show low electrical resistance, with values in the range of several tens of micro-ohms.

## 3.2 Metallographic Analysis of As-joined Cu-cube Joints

Metallographic analysis was carried out to evaluate the cross-sectional morphology of the pressure-less sintered Ag joint between the Cu-cube and the DCB substrate. Light microscopy was first used to examine the overall joint geometry and the continuity of the bonding layer. SEM was then used to observe the sintered Ag layer in more detail.

### 3.2.1 Light Microscopy of the Sintered Ag Layer

Light microscopy was used to evaluate the cross-sectional morphology of the as-joined Cu-cube joints on the DCB test boards. Representative cross-sections are shown in Fig. 7. The images include overview observations at low magnification and detailed views of the sintered Ag layer at higher magnification.

The Ag-based joining layer is clearly visible between the Cu-cube and the copper metallization of the DCB substrate. The layer extends along the observed bonding interface and forms a continuous connection between the two copper surfaces. The Cu-cube, the sintered Ag layer, the lower copper metallization, and the ceramic substrate can be distinguished in the cross-section.

At higher magnification, the joining layer appears as a bright metallic region between the two copper surfaces. Slight local variations in layer thickness are visible along the interface. However, no complete interruption, delamination, or large-scale separation of the joining layer is observed in the presented as-joined cross-sections.

These observations show that the pressure-less sintering process produced a continuous Ag-based bonding layer between the Cu-cube and the DCB substrate in the as-joined condition.

## 3.2.2 SEM Analysis of the Sintered Ag Layer

SEM analysis was performed to examine the sintered Ag layer in more detail. Representative SEM images taken from different positions of the as-joined Cu-cube joint are shown in Fig. 8. The analyzed regions include the left edge region, the central region, and the right edge region of the joint.

The SEM images show that the sintered Ag layer exhibits a metallic porous microstructure. In the edge regions of the joint, shown in Fig. 8(a) and Fig. 8(c), a pronounced porous structure is visible. The Ag network contains interconnected pores and irregularly shaped sintered regions. The pore distribution in these edge regions is not completely homogeneous, and local variations in the morphology of the sintered Ag layer can be observed.

In contrast, the central region of the joint, shown in Fig. 8(b), appears more compact and homogeneous. The SEM images of this region show a much lower amount of visible porosity compared with the edge regions. The sintered Ag layer in the central area appears denser and more uniform in the investigated cross-section.

The comparison of the three positions indicates that the microstructure of the sintered Ag layer is position-dependent within the Cu-cube joint. The edge regions show a more porous and heterogeneous morphology, whereas the central region shows a comparatively dense and uniform structure. This difference is consistent with the light microscopy observation that slight local variations are present along the bonding layer.

Overall, the SEM analysis confirms that the pressure-less sintering process produced a continuous Ag-based joining layer between the Cu-cube and the DCB substrate. The results also show that the internal morphology of the sintered Ag layer is not uniform over the entire bonding area.

## 3.2.3 Die Shear Testing and Fracture Surface Analysis

Die shear testing was carried out to evaluate the mechanical integrity of the as-joined Cu-cube/DCB joints. The measured shear strength values of eight selected samples are shown in Fig. 9. The investigated joints show shear strength values in the range of 69–86 MPa. Most values are located in the range of approximately 70–80 MPa, indicating that mechanically stable joints were formed under the applied pressure-less sintering conditions.

In addition to the individual shear strength values, the box plot in Fig. 9 summarizes the statistical distribution of the selected samples. The distribution shows that the measured values are concentrated in a relatively narrow range, confirming a generally consistent mechanical performance of the as-joined joints.

Based on these results, sample 7, with a shear strength of 79 MPa, was selected as a representative sample for detailed fracture surface analysis after die shear testing. Representative SEM images of the fracture surfaces are shown in Fig. 10. Three different regions were examined on the DCB-testboard side and on the corresponding Cu-cube side.

The overview images show the fracture surfaces after die shear testing. The DCB-testboard side appears partly copper-colored, indicating that areas of the DCB copper metallization are visible after fracture. In contrast, the Cu-cube side shows a more grey surface appearance, which indicates that a larger amount of sintered Ag remained on the Cu-cube side.

The SEM images confirm that residual sintered Ag is present on both fracture surfaces. On the DCB-testboard side, the investigated regions show local residual Ag structures on the surface. Although the overview image appears partly copper-colored, the SEM images show that the surface is not completely free of Ag residues. The Ag residues appear as locally distributed porous and irregular sintered structures.

On the Cu-cube side, the investigated regions show more pronounced residual sintered Ag. The fracture surface exhibits a rough and porous morphology. The residual Ag forms an interconnected sintered network with irregularly shaped pores and locally varying feature sizes. Compared with the DCB-testboard side, the Cu-cube side shows a more continuous coverage of porous Ag residues.

The comparison of the three investigated regions shows local differences in fracture morphology on both sides. Some regions exhibit a relatively open porous structure, while other regions appear finer and more compact. Nevertheless, residual sintered Ag is visible on both the DCB-testboard side and the Cu-cube side in the investigated SEM regions.

The presence of sintered Ag residues on both fracture surfaces indicates that the fracture did not occur exclusively along a single clean Cu/Ag interface. Instead, the fracture path passed partly through the sintered Ag joining layer and partly near the Cu/Ag interface. Therefore, the failure appearance can be described as predominantly cohesive fracture within the porous Ag layer, with local interfacial contributions.

Overall, the die shear and fracture surface results confirm that the pressure-less sintered Ag joints possessed sufficient mechanical performance in the as-joined condition. The representative fracture analysis of sample 7 further shows that the sintered Ag layer participated directly in the failure process during die shear testing.

# 4 Conclusions

In this work, a pressure-less nano-Ag sintering process using an in-situ nano-silver precursor paste was transferred from simplified bulk copper samples to functional DCB test boards. A Cu-cube/DCB test structure was developed to enable four-terminal resistance measurement, metallographic analysis, SEM characterization, and die shear testing of the sintered joint region under application-oriented substrate conditions.

The as-joined Cu-cube/DCB joints showed low electrical resistance in four-terminal measurements, confirming the formation of electrically conductive joints after pressure-less sintering. Metallographic analysis revealed a continuous Ag-based bonding layer between the Cu-cube and the DCB substrate. SEM observations showed a porous sintered Ag microstructure with local non-uniformities, especially near the edge regions of the joint.

Die shear testing showed shear strength values between 69 MPa and 86 MPa for the selected as-joined samples, with most values located in the range of approximately 70–80 MPa. Fracture surface analysis of one selected sample showed residual sintered Ag on both fracture surfaces. The DCB-testboard side appeared partly copper-colored in the overview image but still showed local Ag residues in SEM, while the Cu-cube side showed more pronounced porous Ag residues. These observations indicate predominantly cohesive fracture within the sintered Ag layer, with local interfacial contributions.

Overall, the results demonstrate that the Cu-cube/DCB configuration is a suitable test structure for transferring pressure-less nano-Ag sintering from simplified bulk copper samples to functional DCB test boards. Future work will focus on the long-term reliability of these joints, particularly under thermal cycling conditions.

# Declarations

Funding

This research was conducted in partial fulfillment of a doctoral program jointly funded by MAHLE International GmbH and Chemnitz University of Technology.

Competing interests

The authors declare that they have no competing interests.

**Author contributions**

C.Z. carried out the experimental work, data analysis, figure preparation, and manuscript drafting. M.T. supervised the work and contributed to the conceptual development and revision of the manuscript. Both authors read and approved the final manuscript.

**Data availability**

The datasets generated and analyzed during the current study are available from the corresponding author on reasonable request.

**Acknowledgements**

The authors gratefully acknowledge the support provided by MAHLE International GmbH, Stuttgart, Germany, and the Institute of Materials Science and Engineering at Chemnitz University of Technology. The in-situ nano-silver precursor paste used in this study was kindly supplied by Nano-Join GmbH, Berlin, Germany.

# References

1. Wakamoto K, Namazu T (2024) Mechanical characterization of sintered silver materials for power device packaging: a review. Energies 17:4105. https://doi.org/10.3390/en17164105
2. Cui Z, Jia Q, Wang Y et al (2024) Review on shear strength and reliability of nanoparticle sintered joints for power electronics packaging. J Electron Mater 53:2703–2726. https://doi.org/10.1007/s11664-024-10970-9
3. Li X, Wang L, Gao C, Wang W (2025) Reliability perspective on nano-silver sintering in SiC power modules for space applications. Space Sci Technol 5:0268. https://doi.org/10.34133/space.0268
4. Gain AK, Zhang LC, Quadir MZ (2016) Thermal aging effects on microstructures and mechanical properties of an environmentally friendly eutectic tin-copper solder alloy. Mater Des 110:275–283. https://doi.org/10.1016/j.matdes.2016.08.007
5. Gu M, Nam H, Park S, Shin M, Choa SH (2024) Highly robust, pressureless silver sinter-bonding technology using PMMA combustion for power semiconductor applications. Materials 17:5142. https://doi.org/10.3390/ma17215142
6. Yang Z et al (2024) Microstructure evolution and micromechanical behavior of solvent-modified Cu–Ag composite sintered joints for power electronics packaging at high temperatures. J Mater Res Technol 30:8433–8450. https://doi.org/10.1016/j.jmrt.2024.05.196
7. Xue J, Li X (2024) High-pressure-assisted large-area (> 2400 mm²) sintered-silver substrate bonding for SiC power module packaging. Materials 17:1911. https://doi.org/10.3390/ma17081911
8. Gu M, Liu T (2022) Simulation and experimental study of the multisized silver nanoparticles sintering process based on molecular dynamics. Nanomaterials 12:1030. https://doi.org/10.3390/nano12061030
9. Kim YA, Li Z (2025) Low-temperature sinterable silver paste for die-attachment of wide band gap power electronics. Chem Phys Impact 11:100908. https://doi.org/10.1016/j.chphi.2025.100908
10. Xu Z, Liu X, Li J, Sun R, Liu L (2023) Low-temperature sintering of Ag composite pastes with different metal organic decomposition additions. Materials 16:2340. https://doi.org/10.3390/ma16062340
11. Ye G, Zhang J, Zhang P, Meng K (2024) Sintering mechanism between silver nanoparticles and SiC/Cu plates: a molecular dynamics simulation. Powder Technol 439:119695.

https://doi.org/10.1016/j.powtec.2024.119695
12. Lyu GJ, Zhao SJ, Li BF, He X, Qiao JC (2025) Molecular dynamics simulations on the low-temperature sintering of nano-silver particles for electronic packaging. Powder Technol 464:121224. https://doi.org/10.1016/j.powtec.2025.121224
13. Gu C, Hu X, Yan X, Chen W, Chen J, Lü K, Wang T, Zhang G, Fan J (2025) Interconnection mechanism and strengthening behavior of nano-silver sintered joints for silicon carbide power module packaging: a combined EBSD and nanoindentation study. J Mater Res Technol 38:619–636. https://doi.org/10.1016/j.jmrt.2025.07.135
14. Hong WS, Kim MS (2024) Power cycling reliability with temperature deviation of pressureless silver sintered joint for silicon carbide power module. JOM 76:2763–2771. https://doi.org/10.1007/s11837-024-06398-5
15. Wereszczak AA, Chen BR, Oistad BA (2018) Reflow-oven-processing of pressureless sintered-silver interconnects. J Mater Process Technol 255:500–506. https://doi.org/10.1016/j.jmatprotec.2018.01.001
16. Tian W, Li D, Dang H, Liang S, Zhang Y, Zhang X, Chen S, Yu X (2024) Residual stress and warping analysis of the nano-silver pressureless sintering process in SiC power device packaging. Micromachines 15:1087. https://doi.org/10.3390/mi15091087
17. Zhang C, Tuerpe M, Rabay B (2026) Considerations on joining technology of pressure-less sintering by nano-silver pastes. J Mater Eng Perform. https://doi.org/10.1007/s11665-026-13703-7
18. Zhang C, Türpe M (2026) Investigations on the pressure-less low-temperature sintering process with in-situ nano-silver precursor paste. In: DVS Reports, Vol. 404, EBL 2026 – Electronic Assemblies and Printed Circuit Boards; 2026. p 380. https://doi.org/10.53192/EBL20260380
19. DIN 8514:2006-05 (2006) Brazeability, solderability. DIN Deutsches Institut für Normung e.V., Berlin
20. Zhang C, Tuerpe M, Rabay B (2024) Research on low-temperature sintering by in-situ nano-Ag precursor paste. In: Proceedings of the International Conference on Brazing, Diffusion Bonding and Micro- and Nanojoining, BDB-MNJ 2024; Hangzhou, China

# Figures

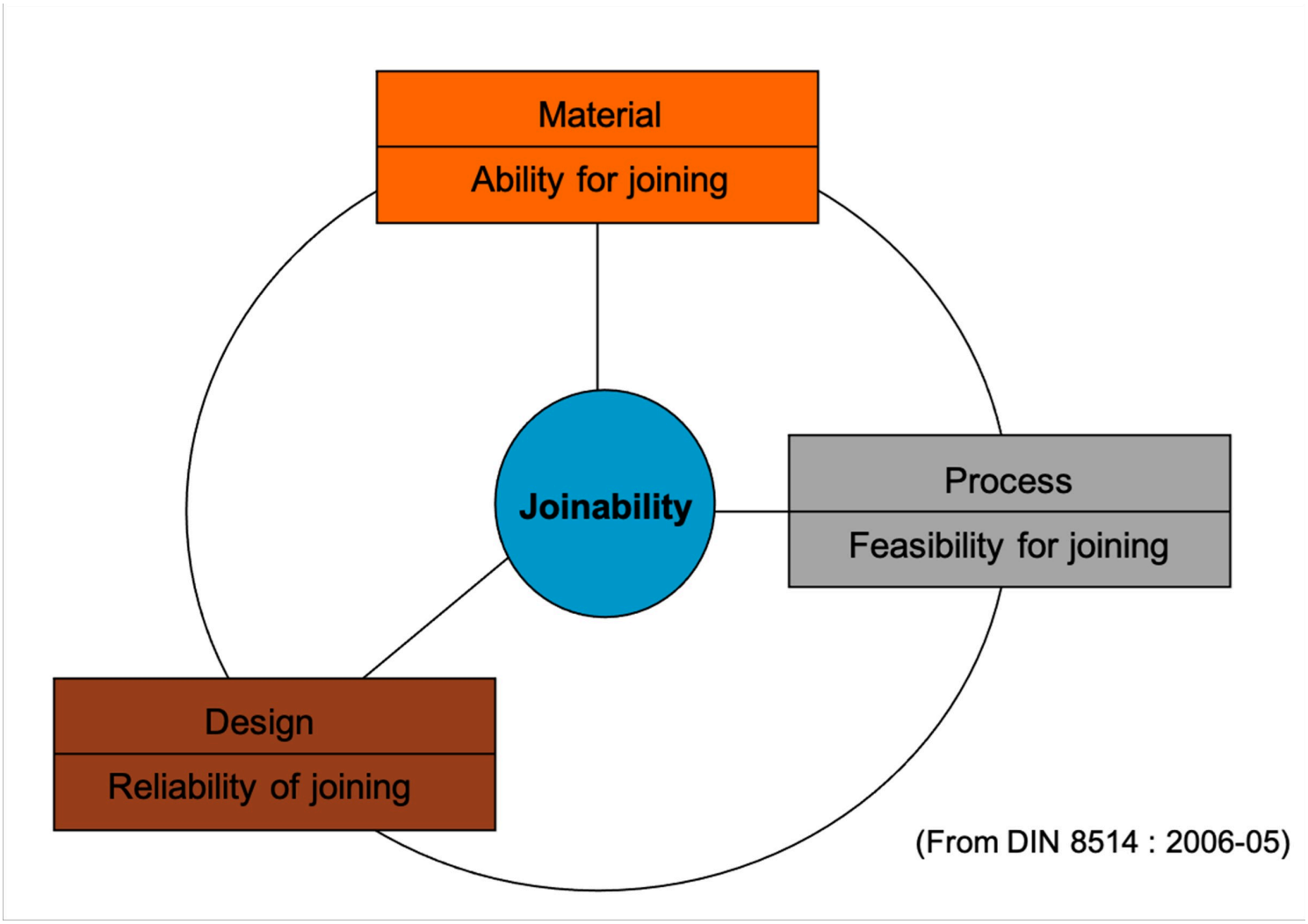



**Figure 1**

Methodological transfer strategy for the development of pressure-less nano-Ag sintering with an in-situ nano-silver precursor paste [18].

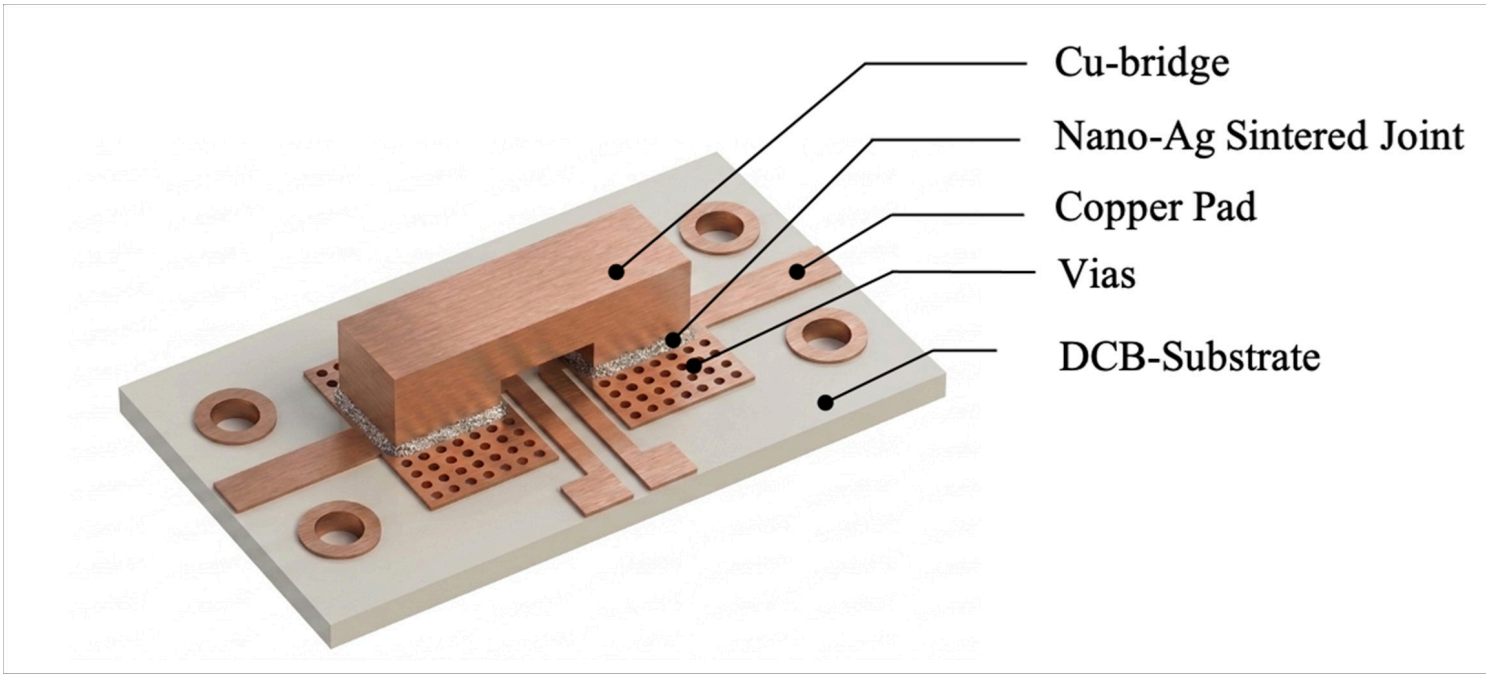



**Figure 2**

DCB test board with Cu-bridge geometry.

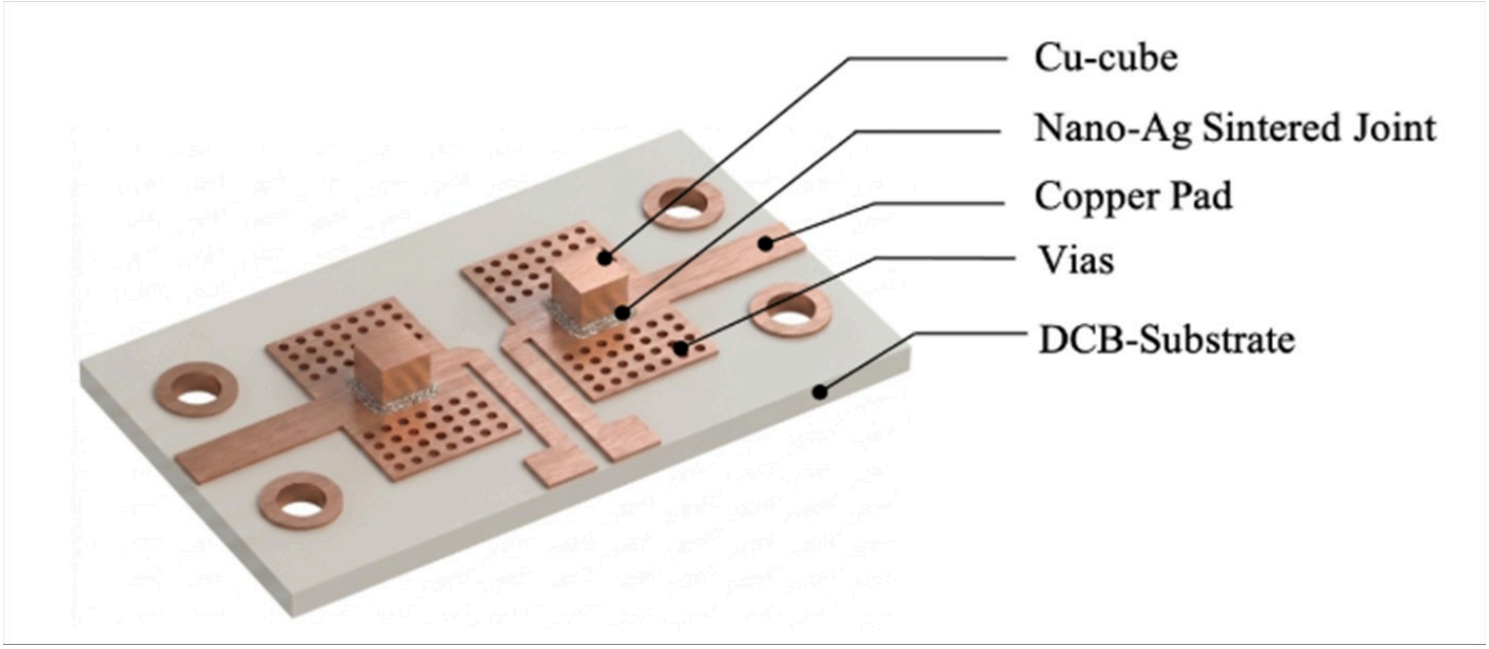



**Figure 3**

DCB test board with Cu-cube geometry, with a Cu-cube size of 2.5 mm × 2.5 mm.

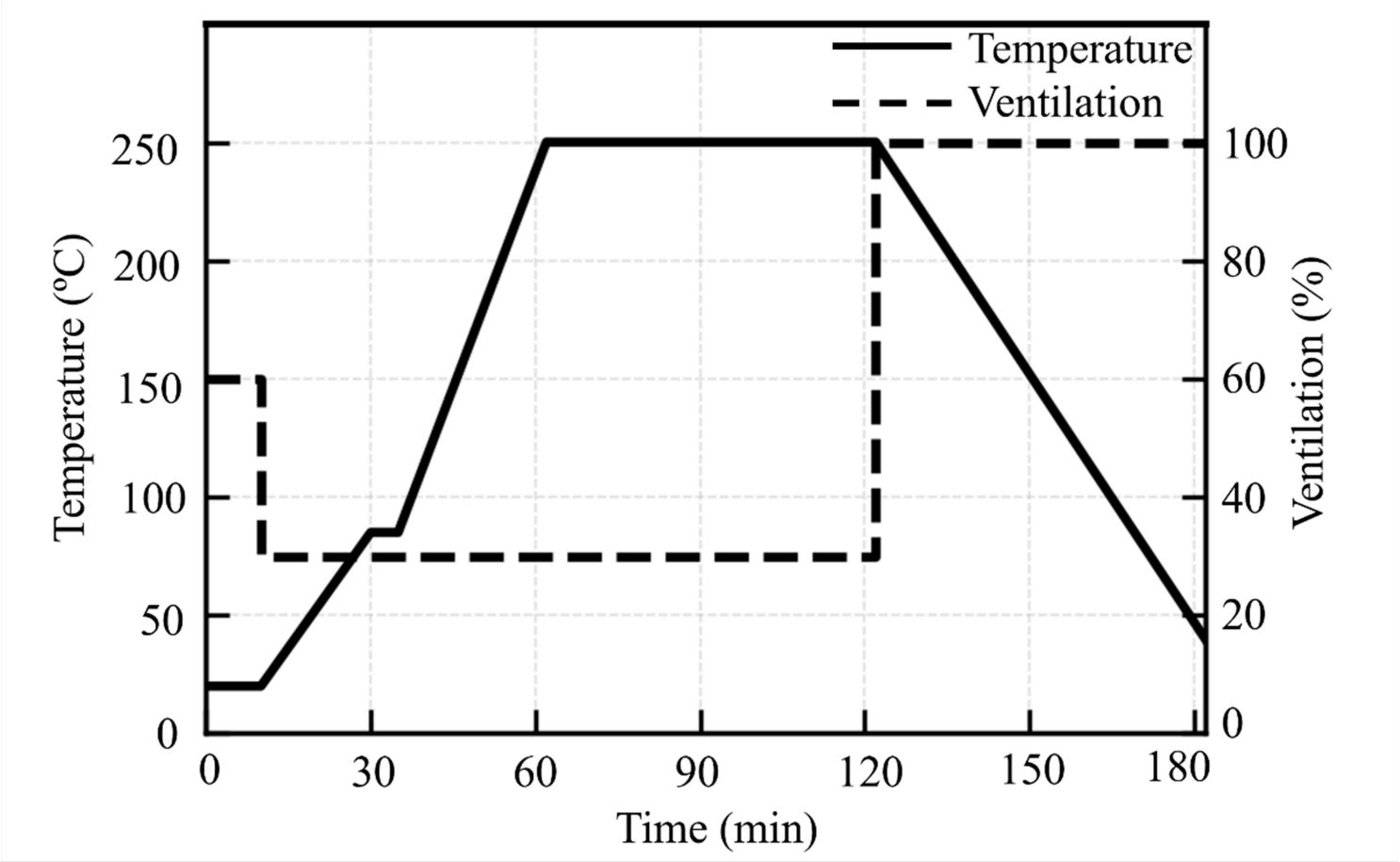



**Figure 4**

Temperature and ventilation profile used for the pressure-less sintering process with the in-situ nano-silver precursor paste [17, 20].

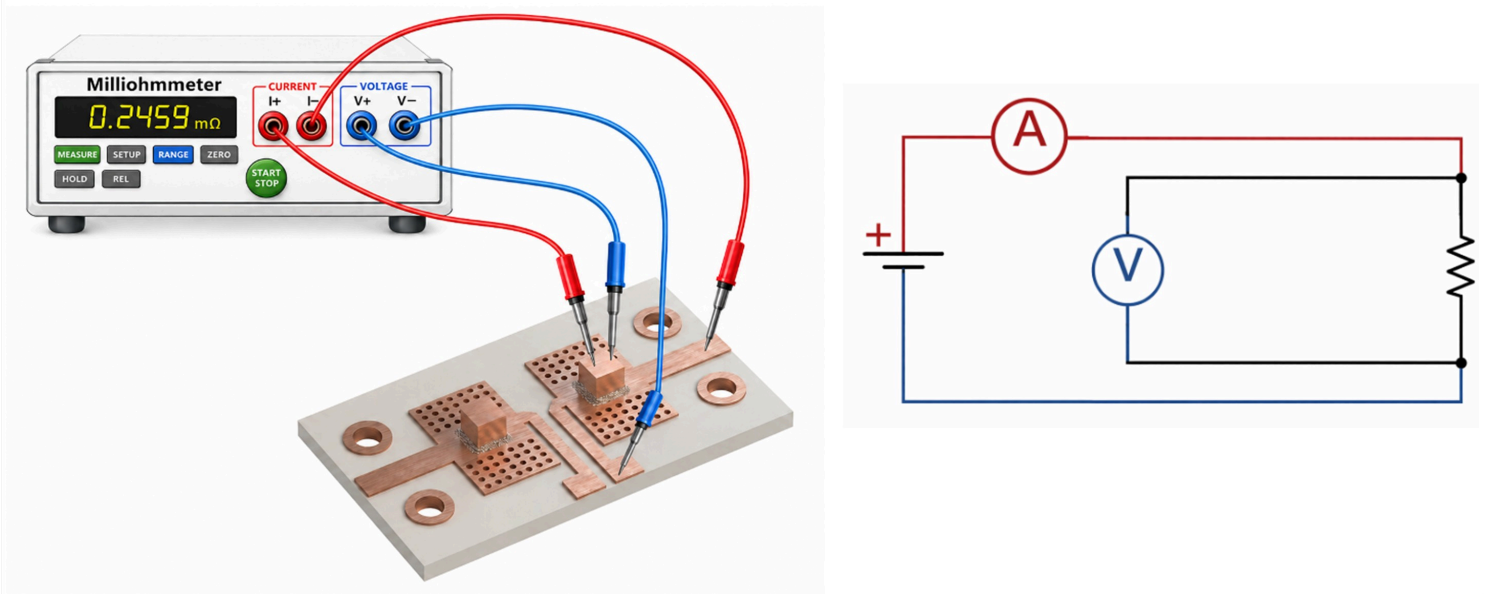



**Figure 5**

Schematic illustration of the four-terminal sensing configuration used for electrical characterization of the Cu-cube/DCB test boards.

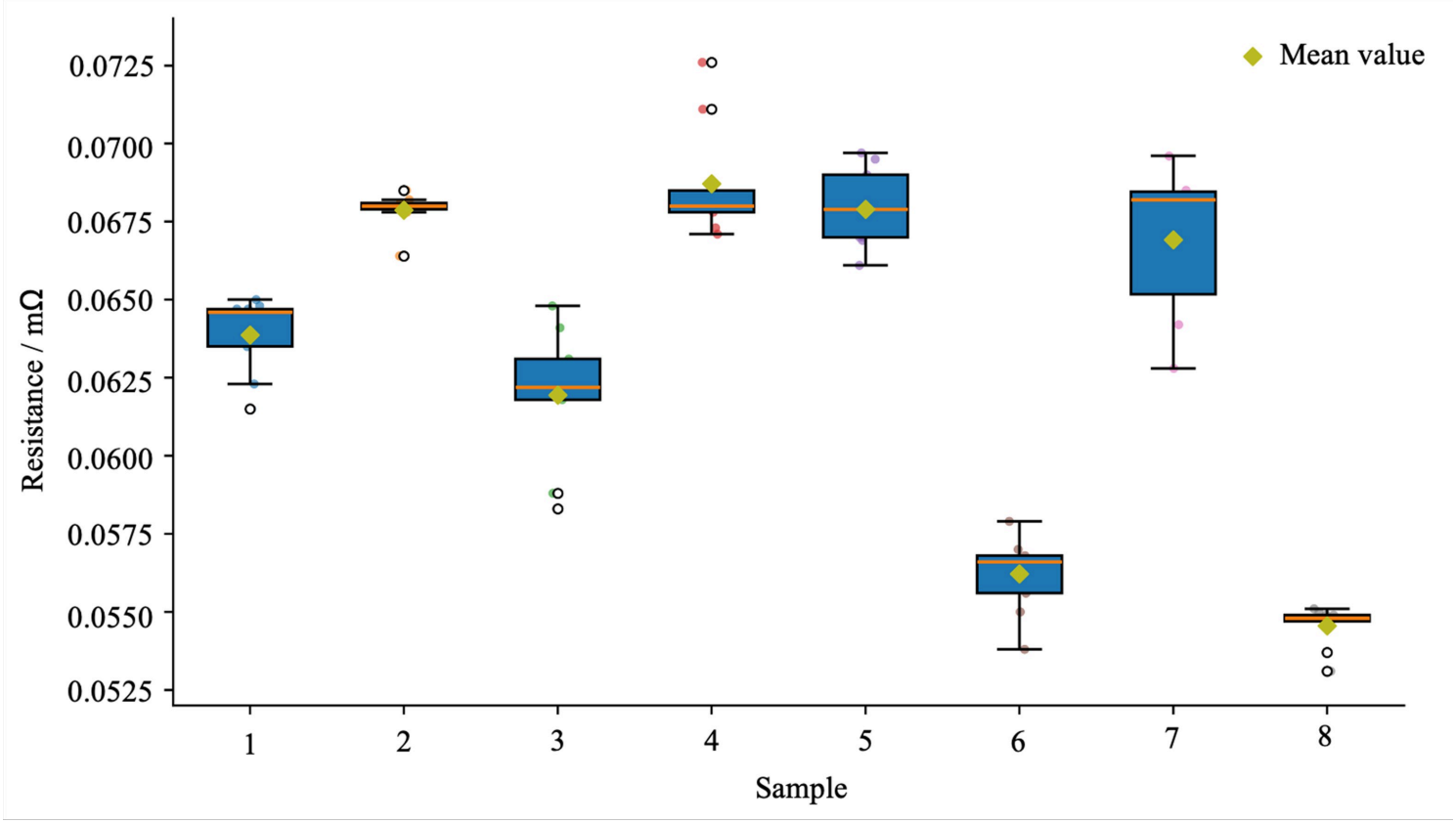



**Figure 6**

Electrical resistance of as-joined Cu-cube (2.5 x 2.5 mm) joints on DCB test boards measured by four-terminal sensing.

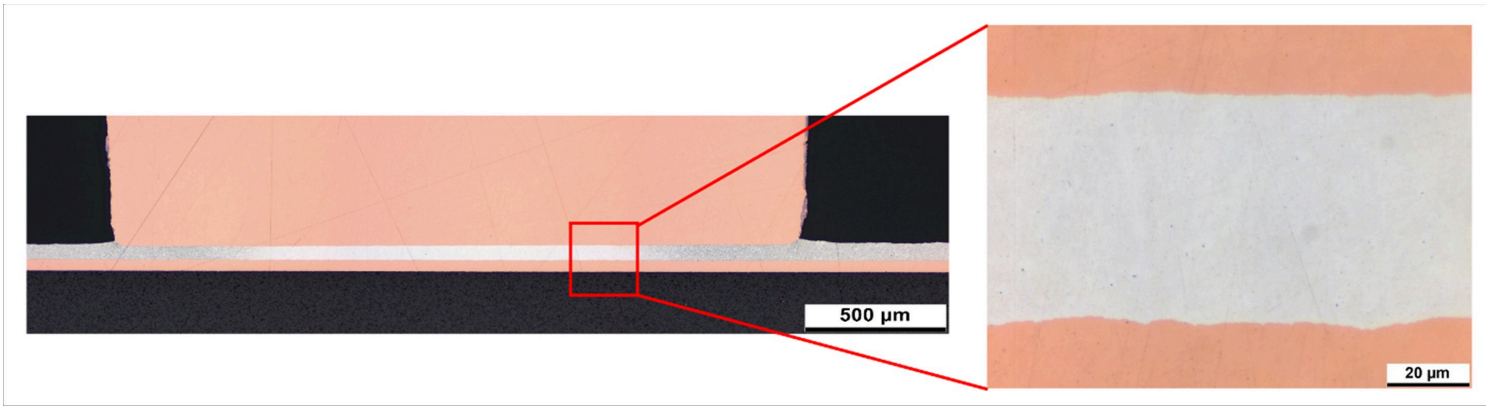



**Figure 7**

Light microscopy cross-sections of the pressure-less sintered Ag joint between Cu-cube (2.5 x 2.5 mm) and DCB substrate in the as-joined condition.

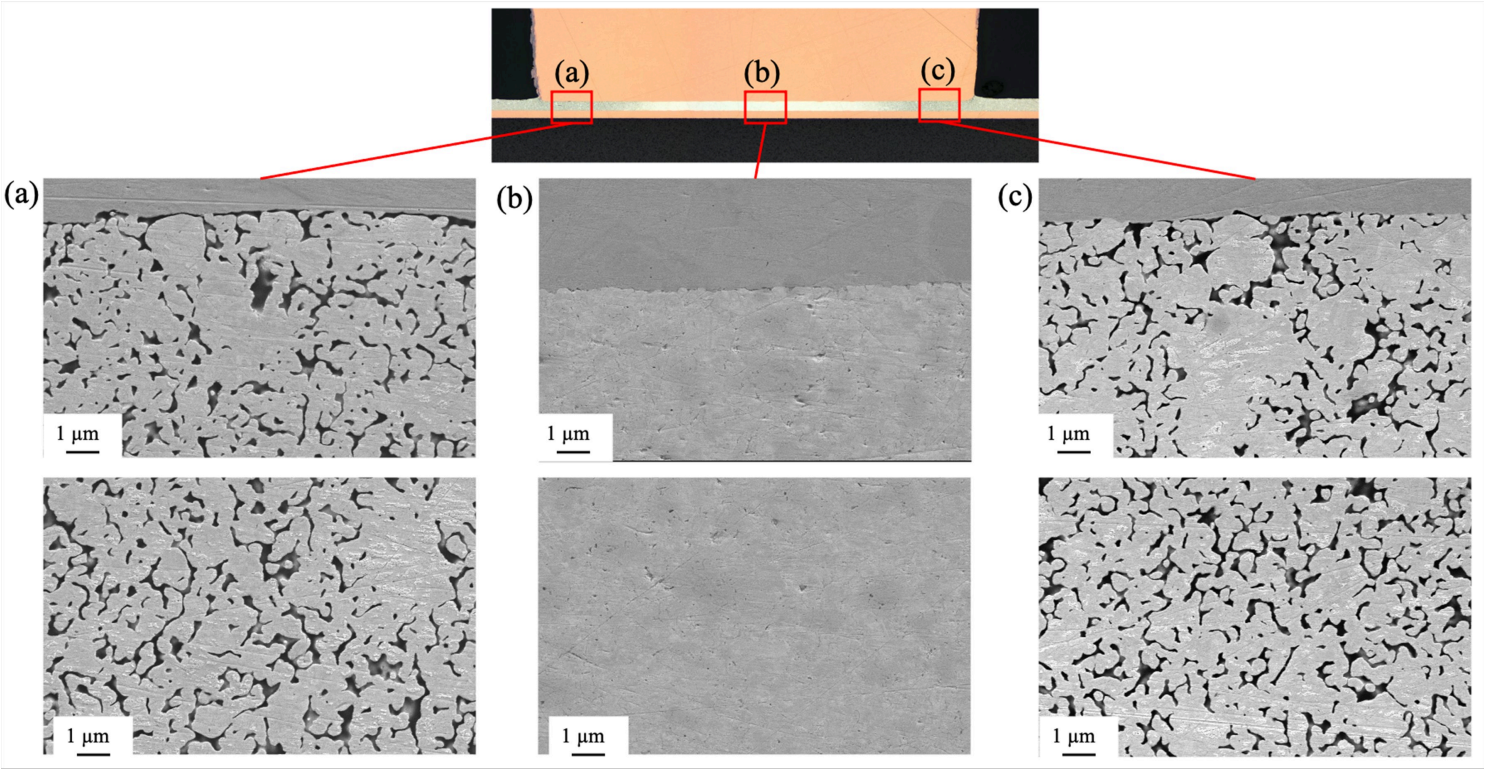



**Figure 8**

SEM images of the sintered Ag layer in the as-joined Cu-cube (2.5 x 2.5 mm)/DCB joint at different positions: (a) left edge region, (b) central region, and (c) right edge region.

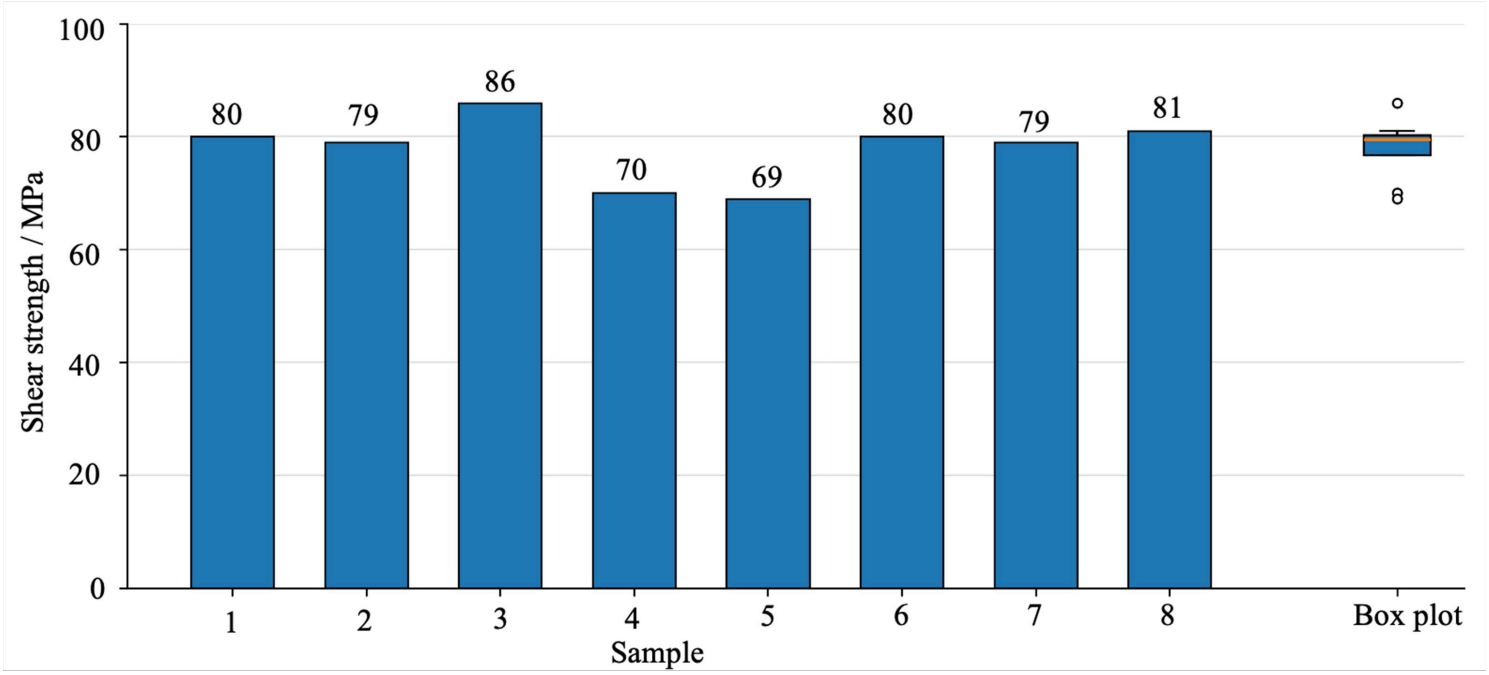



**Figure 9**

Shear strength of eight selected as-joined Cu-cube (2.5 x 2.5 mm)/DCB joints after pressure-less sintering. The bar chart shows the individual shear strength values of the investigated samples, while the

box plot summarizes their statistical distribution.

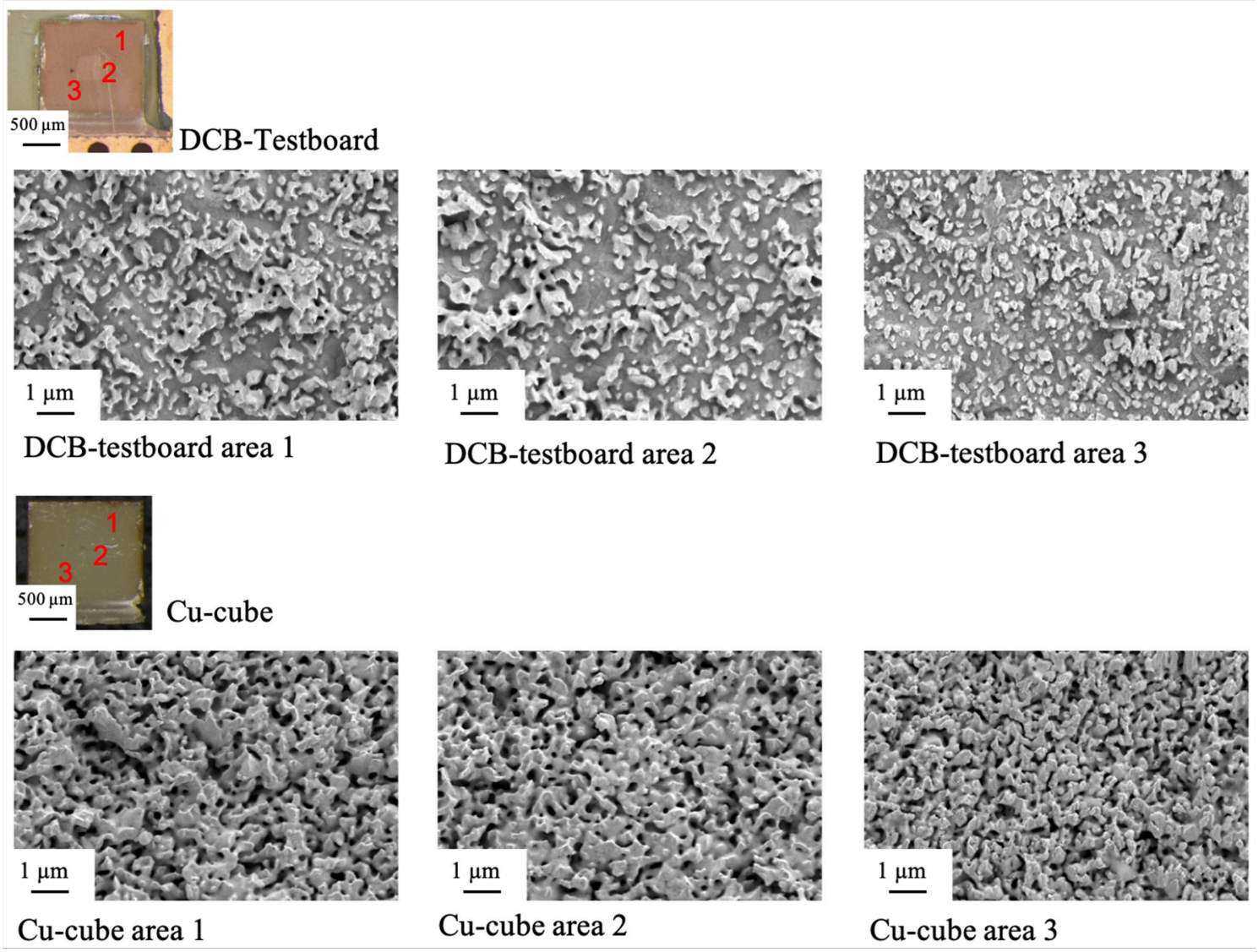



**Figure 10**

Fracture surface analysis of sample 7 after die shear testing. SEM images show three investigated regions on the DCB-testboard side and three corresponding regions on the Cu-cube side.